An atomic hydrogen etching sensor for H_2 plasma diagnostics

Citation for published version (APA):
van Leuken, D. P. J., de Meijere, C. A., van der Horst, R., Banine, V. Y., Osorio, E. A., & Beckers, J. (2021). An atomic hydrogen etching sensor for H_2 plasma diagnostics. *Review of Scientific Instruments*, *92*(6), Article 063518. https://doi.org/10.1063/5.0033518

Document license:
TAVERNE

DOI:
10.1063/5.0033518

Document status and date:
Published: 01/06/2021

Document Version:
Publisher's PDF, also known as Version of Record (includes final page, issue and volume numbers)

Please check the document version of this publication:

• A submitted manuscript is the version of the article upon submission and before peer-review. There can be important differences between the submitted version and the official published version of record. People interested in the research are advised to contact the author for the final version of the publication, or visit the DOI to the publisher's website.
• The final author version and the galley proof are versions of the publication after peer review.
• The final published version features the final layout of the paper including the volume, issue and page numbers.

Link to publication

General rights
Copyright and moral rights for the publications made accessible in the public portal are retained by the authors and/or other copyright owners and it is a condition of accessing publications that users recognise and abide by the legal requirements associated with these rights.

• Users may download and print one copy of any publication from the public portal for the purpose of private study or research.
• You may not further distribute the material or use it for any profit-making activity or commercial gain
• You may freely distribute the URL identifying the publication in the public portal.

If the publication is distributed under the terms of Article 25fa of the Dutch Copyright Act, indicated by the "Taverne" license above, please follow below link for the End User Agreement:

www.tue.nl/taverne

Take down policy
If you believe that this document breaches copyright please contact us at:

openaccess@tue.nl

providing details and we will investigate your claim.

Download date: 04. Oct. 2023

Review of Scientific Instruments

An atomic hydrogen etching sensor for H_2 plasma diagnostics

Cite as: Rev. Sci. Instrum. **92**, 063518 (2021); https://doi.org/10.1063/5.0033518
Submitted: 16 October 2020 . Accepted: 04 June 2021 . Published Online: 16 June 2021

D. P. J. van Leuken, C. A. de Meijere, R. van der Horst, V. Y. Banine, E. A. Osorio, and J. Beckers

ARTICLES YOU MAY BE INTERESTED IN

Two-color interferometer for study of dense low-ionized plasma on the target in high-power pulse linear accelerator
Review of Scientific Instruments **92**, 063519 (2021); https://doi.org/10.1063/5.0045160

Sensitivity improvement of infrared imaging video bolometer for divertor plasma measurement
Review of Scientific Instruments **92**, 063521 (2021); https://doi.org/10.1063/5.0043664

Confronting interatomic force measurements
Review of Scientific Instruments **92**, 063703 (2021); https://doi.org/10.1063/5.0052126

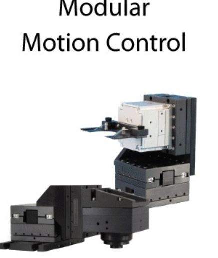

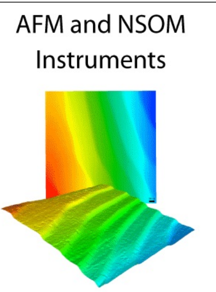

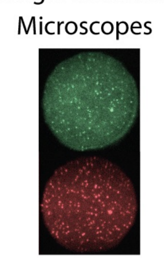

© 2021 Author(s).

Review of Scientific Instruments ARTICLE scitation.org/journal/rsi

An atomic hydrogen etching sensor for H_2 plasma diagnostics

Cite as: Rev. Sci. Instrum. 92, 063518 (2021); doi: 10.1063/5.0033518
Submitted: 16 October 2020 • Accepted: 4 June 2021 •
Published Online: 16 June 2021

View Online
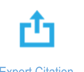
Export Citation
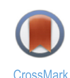
CrossMark

D. P. J. van Leuken,[1,a] C. A. de Meijere,[1,b] R. van der Horst,[1,c] V. Y. Banine,[1,2,d] E. A. Osorio,[1,e] and J. Beckers[2,f]

AFFILIATIONS

[1] ASML, 5504DR Veldhoven, The Netherlands
[2] Department of Applied Physics, Eindhoven University of Technology, P.O. Box 513, 5600 MB Eindhoven, The Netherlands

[a] **Author to whom correspondence should be addressed:** dirk.vanleuken@asml.com
[b] **Electronic mail:** kees.de.meijere@asml.com
[c] **Electronic mail:** ruud.van.der.horst@asml.com
[d] **Electronic mail:** vadim.banine@asml.com
[e] **Electronic mail:** edgar.osorio@asml.com
[f] **Electronic mail:** job.beckers@tue.nl

ABSTRACT

A simple and selective new technique for atomic hydrogen flux measurements in a hydrogen plasma environment is introduced and demonstrated in this work. This technique works by measuring the etching rate of an amorphous carbon film and translating this to an incoming hydrogen radical flux through a well-defined carbon etch yield per radical. Ions present in the plasma environment have a much higher etch yield than radicals do. For that reason, suppression of the ion flux toward the carbon film is crucial to ensure that the observed carbon etch rate is dominated by atomic hydrogen etching. It is demonstrated that this can be achieved using a simple cylindrical pipe (hereinafter "chimney") in which a bend is introduced to enforce ion–wall collisions, neutralizing the ions. The chimney is made out of Macor, a material with low catalytic surface activity, to preserve the incoming atomic hydrogen flux while effectively suppressing ions. Ultimately, the etching sensor is deployed in a radio frequency inductively coupled hydrogen plasma operated at low pressure (1–10 Pa). Atomic hydrogen fluxes are measured and compared with heat flux sensor and vacuum ultraviolet absorption spectroscopy measurements in the same setup. All sensors agreed within a factor 4 in the atomic hydrogen flux range 10^{19} to 10^{21} m^{-2} s^{-1}.

Published under an exclusive license by AIP Publishing. https://doi.org/10.1063/5.0033518

I. INTRODUCTION

The introduction of EUV lithography machines to the field is the next step to keep up with the constant demand for increased computational power and memory capacity.[1] EUV light in these machines has sufficient energy to partially ionize and dissociate the (1–10 Pa) hydrogen background gas that is present in these machines.[2] The generated plasma may interact with optical surfaces, resulting in desired and undesired effects.[3–6] Quantification of the plasma environment in EUV lithography machines is of importance for a better understanding of the plasma material interaction, notably on optical surfaces. Therefore, investigations need to be performed toward the quantification of the individual EUV plasma species: ions, electrons, and radicals. Once the plasma species are quantified in an EUV scanner environment, one can—for example—mimic such an environment, allowing for extensive testing of plasma material interactions under relevant conditions and in an offline fashion. Dynamics of the ions[7–9] and that of the electrons[10–13] have been thoroughly studied for this type of plasma. Yet, the density of neutral hydrogen atoms, which may have dominant importance in the plasma–material interaction, has not yet been thoroughly quantified in (EUV-induced) hydrogen plasmas, partially because of a lack of convenient measurement techniques. In this work, a novel method is presented to measure atomic hydrogen fluxes in a hydrogen plasma environment.

Published under an exclusive license by AIP Publishing

Currently, there are several techniques available to detect atomic hydrogen: vacuum ultraviolet (VUV) absorption spectroscopy,[14,15] the heat flux sensor,[16,17] and Two-photon Absorption Laser Induced Fluorescence (TALIF).[18,19] The VUV absorption technique works by measuring the absorption of Ly-α radiation (121.567 nm) and translating that to the line integrated density of ground-state atomic hydrogen through the known absorption cross section. The TALIF technique works by measuring the re-emitted signal of the hydrogen atom after two photon absorption to determine its density. While both VUV absorption and TALIF techniques are able to measure the atomic hydrogen concentration, complex hardware installation and alignment are required. The reality of the EUV systems would significantly profit from a more simple and compact measurement tool. The heat flux sensor, on the other hand, is a more compact instrument. It measures the heat flux on a surface caused by atomic hydrogen recombination, forming molecular H_2. This heat flux can be translated to a flux of hydrogen atoms through the known amount of heat released upon recombination. This technique has the disadvantage that it is insensitive to low atomic hydrogen fluxes as other heating processes become dominant. Furthermore, the recombination coefficient of the detection surface may also change over time due to degradation, while the technique is sensitive to direct exposure to plasma light as well.

In this work, a novel method, based on an etching sensor, is presented to measure atomic hydrogen fluxes in a hydrogen plasma environment. This is a simple and selective technique, which can be deployed in complex geometries without any feed through requirements. This is something that is not possible with the current sensing techniques.

This paper is outlined as follows: the principle of the etching sensor measurement is explained in Sec. II, and the associated theoretical framework is explained in Sec. III. The experimental setup used in this work is presented in Sec. IV. The experimental results to validate the so-called "chimney" as an efficient ion suppressor are presented in Sec. V. Cross calibrations of the etching sensor against VUV absorption spectroscopy to determine the etching yield of the amorphous carbon detection sample can be found in Sec. VI. Subsequently, the etching sensor is deployed in a hydrogen plasma environment measuring atomic hydrogen fluxes, and the results are presented in Sec. VII. Section VII also includes a comparison with the VUV absorption spectroscopy and heat flux sensor measurements. Finally, conclusions are presented in Sec. VIII.

II. ETCHING SENSOR PRINCIPLE

The etching sensor uses a detection surface of amorphous carbon, which erodes under the exposure of atomic hydrogen. This erosion rate is subsequently translated to an incoming atomic hydrogen flux through the known carbon etch yield per radical. However, in a hydrogen plasma, both atoms and ions are generated. The ions etch much more efficiently than atomic hydrogen does. One can expect a removal probability of 0.1 C atoms per incident H atom[20] for ion(-stimulated) etching, whereas for etching solely by atomic hydrogen, this removal probability is expected at 10^{-4} to 10^{-6} C atoms per incident H atom.[20–22] Thus, suppression of the ion flux toward the carbon sample is required for the technique to work. Therefore, an ion suppressor is developed, which is selective to ions, while preserving the atomic hydrogen flux as much as possible.

The most straightforward way of suppressing ions is to use biased grids, which repel the charged particle flux. However, the cables and feedthroughs required to supply the bias voltage would add much complexity to the system. An alternative is to place a cylindrical pipe (hereinafter "chimney") on top of the carbon film. Incoming ions that collide with the chimney wall will neutralize, forming energetic neutrals. The energy of the formed neutrals is lost by inelastic collision of the chimney wall and scattering with the background gas while traveling down the chimney. Experimental work will point out if sufficient ion suppression and energy loss of the formed neutrals are realized. To enforce the ion–wall interactions, an off-axis chimney design is introduced. The off-axis design will also prevent plasma UV light from reaching the carbon surface, which may have an impact on the etching process. The suppression of plasma UV light was demonstrated successfully in Ref. 23, where it was also shown that the atomic hydrogen flux can be preserved when using a chimney material of low catalytic surface activity. For such materials, atomic hydrogen species are likely to bounce off the surface and travel through the chimney with little chance to be lost. The loss of hydrogen atoms on the surface of the chimney can be characterized by the recombination probability (γ), which is the probability that atomic hydrogen atoms recombine on the surface of the chimney into volatile molecular hydrogen. The recombination probability is material specific. A suitable chimney material should have a low recombination probability. In this work, Macor, which is an easy machinable glass-ceramic, is used as a chimney material. This machinability allows for the introduction of a bend (see Fig. 1) in the chimney. Macor is a dielectric material, which is a composition that mainly consists of silica (SiO_2), magnesium oxide (MgO), and aluminum oxide (Al_2O_3). No literature data were found concerning recombination coefficients of hydrogen radicals on Macor. However, similar recombination coefficients are expected as those for comparable materials such as Pyrex, quartz, and aluminum

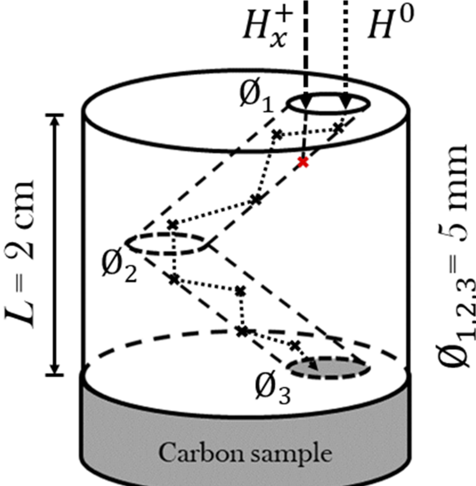

FIG. 1. Schematic of an etching sensor. A bend is introduced in the Macor chimney to enforce particle–wall collision. Ions will neutralize upon collision forming molecular H_2, whereas hydrogen atoms are likely to bounce off the Macor wall and ultimately reach the carbon detection sample. The chimney has a height of L = 2 cm and a tube radius of r = 2.5 mm.

Published under an exclusive license by AIP Publishing

TABLE I. Recombination coefficients for hydrogen radicals on different materials.

Materials	Recombination coefficient (γ)	References
Pyrex	$7.5 \cdot 10^{-4}, 7 \cdot 10^{-4}, 10^{-3}, 5 \cdot 10^{-5}, 5 \cdot 10^{-3}, 9.4 \cdot 10^{-4}$	24–29
Quartz	$5 \cdot 10^{-3}, 5 \cdot 10^{-3}, 7.5 \cdot 10^{-4}$	28–30
Al_2O_3	$5 \cdot 10^{-4}, 6 \cdot 10^{-3}, 2.3 \cdot 10^{-3}$	30–32

oxide. Recombination coefficients for these materials are listed in Table I. For Macor, a recombination coefficient of 10^{-3}to10^{-4} is expected.

In this work, a magnetron sputter-deposited amorphous carbon film (typically, 30 nm thickness) on a 1 in. silicon substrate is used as the target sample (Si–SiO_2–C), as it is known to erode under the exposure of atomic hydrogen.[20–22,33] Carbon sample thicknesses are measured accurately (sub-nanometer resolution) using an *ex situ* spectroscopy ellipsometer. Thickness measurements are performed pre- and post-exposure to determine the erosion rate of the film. A schematic of the etching sensor illustrating its working principle is depicted in Fig. 1.

III. THEORETICAL FRAMEWORK: DIFFUSIVE TRANSPORT IN A CYLINDER OF FINITE LENGTH

In this section, the diffusion and wall recombination of atomic hydrogen in a cylinder of finite length are examined. A schematic representation of the cylindrical geometry can be found in Fig. 2. The pressure as used in the exposures in this work is sufficiently low that atom loss by three-body recombination reactions in the volume can be neglected.[34] Under these conditions, the local H-atom concentration in the cylinder is governed by the balance between diffusion and atom removal by recombination on the chimney surface forming a volatile H_2 molecule. For a diffusive flow in a cylindrical geometry with radial and longitudinal diffusion, the following steady state diffusion equation applies, where gradients in background pressure and temperature are neglected:

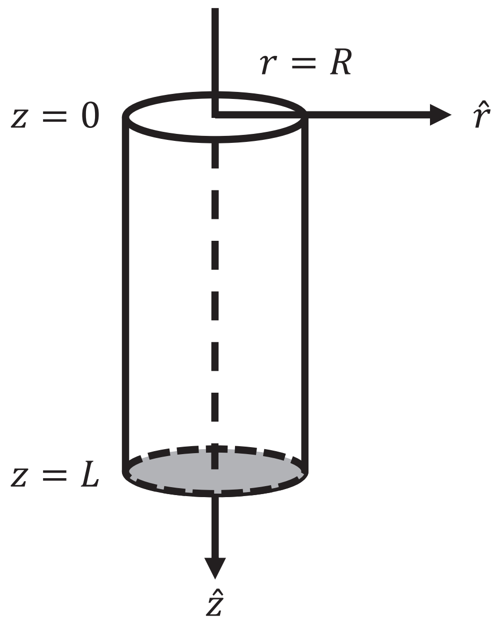

FIG. 2. Schematic presentation of a cylindrical geometry (also referred to as the chimney without bend) with the entrance at $z = 0$, the bottom plate at $z = L$, and radius $r = R$.

$$D\nabla^2 n(r,z) = D\left[\frac{1}{r}\frac{\partial n}{\partial r} + \frac{\partial^2 n}{\partial r^2} + \frac{\partial^2 n}{\partial z^2}\right] = 0. \tag{1}$$

Here, r is the radial distance, z is the longitudinal distance, n is the particle concentration, and D is the diffusion coefficient. The boundary conditions on the solution of the partial differential equation (1) are given by

$$n(r,0) = n_0, \tag{2}$$

$$\frac{\partial n}{\partial r}(0,z) = 0, \tag{3}$$

$$\frac{\partial n}{\partial r}(R,z) = -n(R,z)/\delta R, \tag{4}$$

$$\frac{\partial n}{\partial z}(r,L) = -n(r,L)/\delta' R, \tag{5}$$

where (2) imposes a flat concentration distribution at the entrance and (3) states that the radial concentration distribution has a maximum on the z axis. In (4) and (5), Fick's law of diffusion is used in the radial and longitudinal direction, respectively. Here, $\delta^{(\prime)} = \frac{4D}{\gamma^{(\prime)} v_{th} R}$, where γ and γ' represent the recombination coefficient on the cylinder wall and the end plate, respectively, and v_{th} represents the thermal velocity $v_{th} = \sqrt{\frac{8k_bT}{\pi m_H}}$, with m_H being the atomic hydrogen mass. The solution to Eq. (1) that satisfies boundary conditions (2)–(5) is given by

$$n/n_0 = 2\sum_{i=1}^{\infty} \frac{\left[\sinh\left(\alpha_i \frac{L-z}{R}\right) + \delta'\alpha_i \cosh\left(\alpha_i \frac{L-z}{R}\right)\right] J_0\left(\alpha_i \frac{r}{R}\right)}{\alpha_i(1+\delta^2\alpha_i^2)J_1(\alpha_i)[\sinh(\alpha_i L/R) + \delta'\alpha_i \cosh(\alpha_i L/R)]}, \tag{6}$$

where α_i's are the roots of the equation $J_0(\alpha_i) = \alpha_i J_1(\alpha_i)$. Here, J_0 and J_1 are Bessel functions of the first kind. This equation is used for fitting of the experimentally obtained atomic hydrogen transmission through the chimney using $\delta^{(\prime)}$ as the fitting parameter.

A. Diffusion in the transitional regime

The nature of gas flow through a cylindrical geometry changes with gas pressure, separating the pressure dependence of the flow into three regimes. These regimes can be defined by the Knudsen number ($Kn = \lambda/R$), which is a dimensionless number defined as the ratio between the species' mean free path (λ) and the characteristic length scale of the system, in this case the radius (R) of the chimney. The three flow regimes are as follows: (I) *free molecular flow* ($Kn \gg 1$), gas dynamics are dominated by molecular collisions with the chimney walls; (II) *continuum flow* ($Kn \ll 1$),

Published under an exclusive license by AIP Publishing

inter-molecular collisions are more frequent than wall collisions; and (III) *transitional flow* ($Kn \sim 1$), where both intermolecular and wall collisions influence the flow characteristics. In this work, the operation conditions are such that the atomic hydrogen's mean free path has a similar length scale as the diameter of the chimney pipe (*transitional flow*, $Kn \sim 1$). In this case, the diffusion coefficient is typically described by the Bosanquet relation[35,36]

$$\overline{D} = \left(\frac{1}{D_k} + \frac{1}{D_b}\right)^{-1}, \tag{7}$$

which is also used in this work to derive the recombination coefficient ($\gamma^{(')}$) from the fitting parameter $\delta^{(')}$ in Eq. (6). This reciprocal additive relation has a term that describes diffusion in case wall collisions are dominant by the Knudsen diffusion coefficient[37] (*free molecular flow*, $Kn \gg 1$) $D_K = \frac{2Rv_{th}}{3}$, where v_{th} is the thermal velocity. The second term in the Bosanquet relation describes bulk diffusion (*continuum flow*, $Kn \ll 1$) $D_b = \frac{3k_bT}{8p\sigma_{12}^2}\left(\frac{k_bT}{2\pi}\left(\frac{1}{m_H} + \frac{1}{m_{H_2}}\right)\right)^{1/2}$,[38] with m_{H_2} being the molecular hydrogen mass, p being the gas pressure, and σ_{12} being the H–H_2 collision cross section.

IV. EXPERIMENTAL SETUP

In this section, the experimental setup is presented and discussed. A schematic representation of the setup can be found in Fig. 3. This setup includes two atomic hydrogen sources: the hydrogen radical generator (HRG),[39] which produces solely atomic hydrogen, and the RF ICP plasma source,[40] which produces both hydrogen ions and atoms. The HRG is a collective of filament, gas nozzle, and power supply. It has a tungsten (W) filament with 0.25 mm diameter that is wound up five times, creating a helical spring with an inner diameter of 1.5 mm. During operation, the filament is heated electrically, typically, up to temperatures of 1600–1950 °C as measured with a pyrometer.

The second atomic hydrogen source is a radio frequency (13.56 MHz) ICP (CCR Technology GmbH), generating both hydrogen atoms and ions. The plasma source is situated on top of the vacuum vessel where a tungsten mesh with 10 mm grid size separates the source from the underlying vacuum chamber. The generated plasma can diffuse through the grid and expand in the underlying chamber. This underlying chamber is a stainless steel vacuum vessel in which the experiments are conducted. The vessel is cylindrical and has a diameter of 25 cm and a height of 30 cm. There are two quartz viewports on opposite sides in the vessel walls, allowing for the installation of the vacuum ultraviolet (VUV) absorption spectroscopy setup or the heat flux sensor. Installations of the VUV setup require both ports: one for the light source and one for the spectrometer (McPherson Model 234/302). When installed, the light path from the source to the spectrometer is ~30 cm.

The heat flux sensor requires a single port for installation. A retractable arm with, at the end, the heat flux sensor is inserted in the vacuum vessel via one port. The retractable arm allows for positioning of the heat flux sensor in the center of the vacuum vessel.

Placing of the etching sensor is typically done on the bottom of the vacuum vessel directly below the two atomic hydrogen sources. Here, it is distanced 20 cm from the radical generator and 30 cm from the plasma source. It is possible to place the etching sensor right below the light path of the VUV setup, which is distanced roughly 10 cm from the bottom of the vessel.

To allow for ion flux measurements, a retarding field energy analyzer (RFEA) can be installed and placed on the bottom of the vacuum vessel. In this study, the Impedans Semion Single Sensor RFEA is used, which, for the bias grids used, has a lower detection limit of $\sim 10^{11}$ cm^{-2} s^{-1}. The pressure in the vessel is maintained using a PID controller, which regulates the mass flow controller, to keep constant species fluxes throughout exposure.

Measurements of the carbon film thickness are done *ex situ* using a J.A. Woollam M-2000 ellipsometer. Carbon film thickness determination is done using the already available modeling capabilities of the Woollam ellipsometer (CompleteEASE software package) with the carbon film thickness as the only fitting parameter. The carbon samples are manufactured at Philips innovation services.[41] Manufacturing of the samples is done via magnetron sputtering, a technique in which a radio frequency argon plasma is generated and the energetic ions bombarded a carbon sample. As a result, carbon atoms are ejected and deposited on a 1 in. silicon substrate. Typically, a carbon film of 30 nm thickness is grown on the substrate.

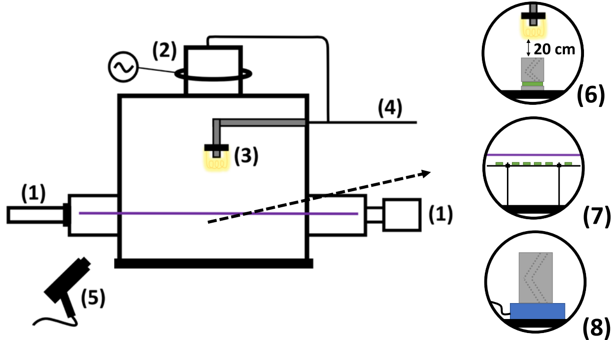

FIG. 3. Schematic representation of the experimental setup: (1) vacuum ultraviolet absorption spectroscopy setup, (2) RF (13.56 MHz) ICP source, (3) hydrogen radical generator, (4) H_2 supply, (5) pyrometer, (6) etching sensor, and (7) stainless steel strip (300 × 10 mm^2) with carbon samples on top, placed right below the UV beam path. (8) The RFEA with the chimney on top.

V. EXPERIMENTAL VALIDATION OF THE ATOMIC HYDROGEN FLUX SENSOR FOR PLASMA DIAGNOSTICS

The first validation step is to check whether the chimney is able to suppress ions to a greater extent than it does to radicals. This is a requirement for the etching sensor to work as ions etch the carbon film more efficiently than atomic hydrogen does. Next to that, in this step, the atomic hydrogen transmission through the chimney is determined, which is needed to translate the incoming atomic hydrogen flux at the etching sample to an atomic hydrogen flux at the entrance of the chimney. A rough estimation, based on expected particle fluxes and etch yields, suggests that the ion flux should be suppressed by at least three orders of magnitude more than the radical flux. In this section, the experimentally obtained transmission of hydrogen atoms and ions through a Macor chimney in the

Published under an exclusive license by AIP Publishing

transitional flow regime ($Kn \sim 1$) is presented. This is done for a series of chimneys with varying length and diameter with a geometry as presented in Fig. 2 and the chimney with bend; see Fig. 1. This is done for both geometries to get a better understanding of plasma species transport in small geometries. Ultimately, it is investigated whether sufficient ion suppression is achieved such that etching of the carbon sample is dominated by atomic hydrogen.

A. Atomic hydrogen transmission through Macor chimney

The transmission of atomic hydrogen through the Macor chimney is determined by measuring the erosion rate of an amorphous carbon film by atomic hydrogen exposure at the entrance and at the exit of the chimney. In Fig. 2, this would be at $z = 0$ and $z = L$. To facilitate this, an extra carbon sample is placed on top of the chimney near the entrance. The transmission is then given by the ratio in erosion rates. This is under the assumption that the atomic hydrogen concentration is linearly proportional to the carbon etch rate and that the etch yield is equal for both samples at the exit and at the entrance of the chimney. Temperature differences of the samples could result in different measured etch yields. For that reason, temperature measurements are performed in the surrounding of the samples using a thermocouple, which showed a constant temperature of about 40 °C.

Atomic hydrogen is generated using the radical generator, which is operated at $T = 1900$ °C and suspended in a 10 Pa H_2 environment. Radicals are generated at the surface of the filament and have to travel at least 20 cm before reaching the entrance of the chimney; plentiful collisions take place along the way as the mean free path at this pressure is in the order of a millimeter. Atomic hydrogen species are therefore assumed to be in thermal equilibrium with the hydrogen molecules (i.e., with the background gas).

Ex situ spectroscopic ellipsometric measurements are performed to measure the thickness of the etching sample pre- and post-exposure. Flat etching profiles were observed, which one would expect from an evaluation of Eq. (6) for a chimney made out of a material with a low recombination coefficient, such as Macor. As a rule of thumb, at least 5 nm of carbon should be etched away to allow for sufficient accurate determination of etching rates. Experimentally obtained atomic hydrogen transmission for chimneys without bend of various dimensions is presented in Fig. 4. As expected, higher atomic hydrogen transmissions are observed for larger chimney diameters and lower transmissions for increasing chimney lengths both due to a changing number of radical-wall collisions. In general, relatively high (>65%) atomic hydrogen transmissions are observed, which was one of the chimney requirements.

In the same manner, the atomic hydrogen transmission for the chimney with bend (see Fig. 1) was found to be 0.85 ± 0.06.

In addition, the experimental data as presented in Fig. 4 are fitted using Eq. (6) with δ and δ' as fitting parameters for $z = L$, $r = 0$, and the diffusion coefficient according to the Bosanquet relation [Eq. (7)]. With atomic and molecular hydrogen masses obtained from Ref. 42, cross sections from Ref. 34, and T set to thermocouple readings in the vicinity of the chimney (≈350 K), one obtains a recombination coefficient for Macor of $\gamma_{Macor} = (6.0 \pm 2.6) \cdot 10^{-4}$ that is found to be comparable with literature values for similar materials; see Table I. Furthermore, the recombination coefficient of the bottom plate, carbon, was found to be $\gamma_{Carbon} = (9.5 \pm 3.8) \cdot 10^{-3}$. It followed from inspection of Eq. (6) that for the geometries and operation conditions used, the atomic hydrogen concentration in the chimney is sensitive to both the bottom plate and the wall material.

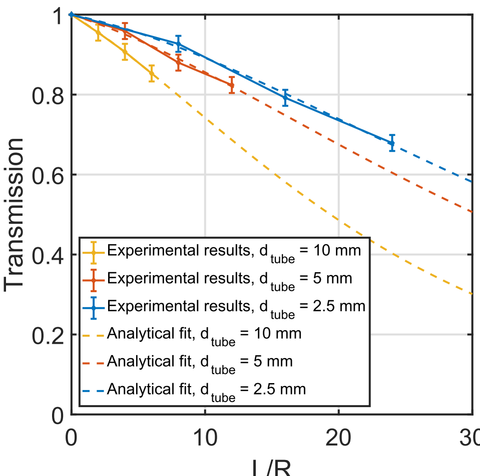

FIG. 4. Experimentally obtained atomic hydrogen transmission for the Macor chimney without bend (Fig. 2 for geometry). The transmission is defined as the ratio in the carbon etch rate at $z = 0$ and $z = L$ in a 10 Pa H_2 environment. Only atomic hydrogen species, generated by using the HRG, were present during exposures. The data are fitted using Eq. (6) for $z = L$ and $r = 0$ with δ and δ' as fitting parameters.

B. Hydrogen ion transmission through Macor chimney

In this subsection, experimentally obtained ion transmissions are presented and discussed. Hydrogen ion species are generated using the plasma source that is situated on top of the vessel; see Fig. 3. Ions with energies of 5–10 eV and fluxes around 10^{14} cm^{-2} s^{-1} are measured at the bottom of the vacuum vessel when operating the plasma source at 500 W and having aH_2 pressure of 5–10 Pa. These measurements are performed using a retarding field energy analyzer (RFEA). The RFEA can also be used to determine the ion transmission through the Macor chimney. This is done by measuring ion fluxes with and without the chimney on top of the RFEA. The ratio in ion flux is taken as the ion transmission. RFEA measurements are performed at the bottom of the vacuum vessel for chimneys with a maximum height of 3 cm. The ion flux showed no longitudinal gradients in this region, as measured by using the RFEA. Experiments have shown that a minimum ion transmission of 1% is achieved for a chimney length of 30 mm (geometry as in Fig. 2). This is observed for all three diameters (2.5, 5, and 10 mm), which is expected behavior for the case that ions are accelerated into the chimney. For this to happen, the plasma sheath has to span over the chimney entrance; this requires the plasma sheath thickness to be larger than the chimney entrance diameter. A plasma sheath is a layer in a plasma, which has a greater density of positive ions and hence an overall excess positive charge, which balances an opposite negative charge on the (chimney) surface, which is in contact with

Published under an exclusive license by AIP Publishing

TABLE II. Carbon etching yield (Y) under atomic hydrogen exposure calculated as prescribed in Eq. (9) where subscripts "pre" and "post" refer to the moments in time the VUV line integrated density was measured. Next to that, the corresponding line-integrated density and line-averaged etch rate are presented in this table.

P (Pa)	Y_{pre} [a]	Y_{post} [a]	Line-averaged etch rate (nm/h)	Line-integrated density pre (m^{-2})	Line-integrated density post (m^{-2})
5	$2.42 \cdot 10^{-5}$	$3.83 \cdot 10^{-5}$	0.19	$1.202 \cdot 10^{17}$	$7.585 \cdot 10^{16}$
10	$1.40 \cdot 10^{-5}$	$1.93 \cdot 10^{-5}$	0.26	$2.880 \cdot 10^{17}$	$2.089 \cdot 10^{17}$

[a]Removed C atoms per incident H atom.

the plasma. The potential drop across the plasma sheath accelerates the ions over the sheath and potentially into the chimney. To estimate the sheath thickness, Langmuir probe measurements are performed, which indicated a sheath thickness of a few millimeters ($n_e \approx 10^9$ cm^{-3} and $T_e \approx 2$ eV) for the practiced operation conditions. These dimensions are comparable with chimney entrance diameter. It is expected that the plasma sheath does not span over the chimneys entrance but rather dips in the chimney. At this point, the ion transmission would be dependent on the tube diameter, as a varying fraction of the ions are accelerated toward the chimney wall. This is not observed; however, the plasma sheath thickness may increase in the chimney, resulting in ballistic ions. This is valid for the case that in the chimney, the electron density decays faster than the electron temperature does. This could explain similar transmission curves only if this process takes place in the very beginning of the chimney.

The same transmission measurements are performed for the chimney with bend, as presented in Fig. 1. It was not possible to measure an ion flux when the chimney with bend is on top of the RFEA, meaning that there was no signal above the noise level, which implies that the incoming ion flux of 10^{14} cm^{-2} s^{-1} is suppressed by at least three orders of magnitude. This is at least one order of magnitude more than for the regular straight chimney, showing that the introduction of the bend in the chimney successfully enforced ion wall collisions and consequently enhanced ion suppression.

C. Macor chimney as ion suppressor

It has been shown that the ions can be suppressed to a greater extent than the radicals can be using the Macor chimney. Yet, the fundamental question remains: when is the ion suppression sufficient such that etching of the carbon sample is dominated by hydrogen radicals. To answer this question, the carbon etch rate is measured in a plasma environment where ions and radicals are present and in an environment with only hydrogen radicals generated by using the HRG. The etch rate as a function of chimney length is compared for both environments. In case a similar trend in the etch rate as a function of chimney length is observed for exposures in both environments, it would suggest that the carbon etching is governed by the hydrogen radicals. If ions, plasma light, or energetic atomic hydrogen neutrals formed after energetic ion neutralization would contribute to the erosion of the carbon film in the plasma environment, a faster etch rate decrease as a function of chimney length is expected with respect to the situation where only atomic hydrogen contributes to the erosion of the carbon film.

The results of these exposures are presented in Fig. 5. The tube length on the horizontal axis refers to the length of the chimney without bend. In two cases (I and II in Fig. 5), a chimney with bend is placed on top of the chimney without bend. In case the tube length is zero, it means that only the chimney with bend was used. The radii of the chimneys that are placed on top of each other are matched, $r = 2.5$ mm. As a reference, a third dataset (III in Fig. 5) is added, which presents etch rates in the plasma environment where only the chimney without bend with radius $r = 1.25$ mm is used. Again, the temperature near the chimney was measured using a thermocouple; for both sources, a temperature of 40 °C was measured. Experimental datasets I and II in Fig. 5 are fitted with an exponential function, $ER = a \cdot \exp[-x/\lambda]$, where x represent the chimney's tube length and a and λ are fitting parameters. Both sources were operated at the same H_2 background pressure of 5 Pa. Similar decay lengths (λ) are observed, suggesting that sufficient ion and plasma light suppression is achieved such that carbon etching is dominated by atomic hydrogen only. Furthermore, it also suggests that energetic atomic hydrogen neutrals, which could be formed after neutralization of energetic ions, do not play an important role in the carbon etching process. Next to that, flat etching profiles are observed for all

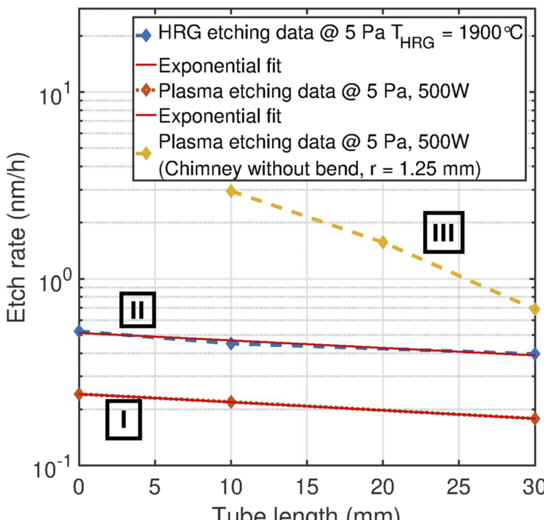

FIG. 5. Carbon etching rate as a function of chimney tube length for three cases: (I) in a plasma environment using a chimney with bend (Fig. 1, $r = 2.5$ mm) placed on top of a chimney without bend (Fig. 2, $r = 2.5$ mm). The chimney tube length on the horizontal axis refers to the length of the chimney without bend: zero means only chimney with bend is used. (II) Similar to (I) but in an environment with only atomic hydrogen species generated by using the HRG. (III) Carbon etch rates in a plasma environment using only the chimney without bend (Fig. 2, $r = 1.25$ mm).

Published under an exclusive license by AIP Publishing

exposures where a chimney with bend is used. This can be expected from an evaluation of Eq. (6) for a Macor chimney, also hinting that etching is dominated by radicals only. Both observations, i.e., similar carbon etch rate decay (λ) and etch profile when comparing exposures of HRG and plasma source, are not observed when only using a chimney without bend, suggesting that ions still contribute to the erosion of the carbon sample. This can be clearly observed in Fig. 5 by comparing datasets I and II with III. A stronger decrease in the etch rate is observed as a function of chimney tube length for the case where only the chimney without bend is placed on top of the carbon sample (III in Fig. 5). Hence, the off-axis chimney design is needed to realize sufficient ion suppression. Furthermore, both sources show comparable carbon etch rates in the situation where etching is governed by atomic hydrogen species only. This indicates that plasma source and HRG generate similar amounts of atomic hydrogen.

VI. CARBON ETCHING SENSOR CROSS CALIBRATIONS

Atomic hydrogen fluxes are obtained by translation of carbon etching rates under atomic hydrogen exposure to an incident atomic hydrogen flux. The relation between the carbon etching rate and incident atomic hydrogen flux (Γ_H) is given as follows:

$$\Gamma_H = \frac{ER \cdot \rho_C \cdot N_A}{Y \cdot M_C}, \tag{8}$$

where ER represents the carbon etch rate, ρ_C is the carbon density, N_A is Avogadro's constant, and M_C is the molar mass of carbon. The quantities ER, ρ_C, N_A, and M_C are used to calculate the amount of removed carbon atoms per unit of surface area per unit of time. This is subsequently translated to an incoming atomic hydrogen flux using the yield (Y), defined as the amount of carbon atoms removed per incident hydrogen atom. The etching yield can be found in the literature or determined by cross calibrations using established detection techniques. The literature study showed a wide range of yield values (10^{-4} to 10^{-6}), which could vary orders of magnitude depending on the type of carbon.[20–22,33] For that reason, cross calibrations are preferred and performed to determine the etch yield.

In this study, vacuum ultraviolet (VUV) absorption spectroscopy is used for cross calibration of the carbon etching sensor to retrieve the carbon etching yield. The VUV absorption spectroscopy technique measures line integrated densities. In order to spatially resolve this line integrated measurement, a density profile needs to be plugged in. The density profile right below the line beam path is obtained experimentally by measuring carbon etch rates under atomic hydrogen exposure at different positions along the VUV beam light path. This is done by placing 5×5 mm^2 carbon samples on a 300×10 mm^2 stainless steel strip, which is then placed right below the VUV light path; see Fig. 3. The influence of the presence of the carbon samples including the strip below the VUV beam on the measured line integrated density is neglected.

From these measurements, the carbon etch rate profile $[ER(x)]$ is obtained, which is used to determine the line integrated etch rate, which, in turn, is used to derive the yield (Y) using the following relation:

$$\int_0^L ER(x)dx = Y\frac{v_{th}M_C}{4\rho_C N_A}\int_0^L n(x)\ dx, \tag{9}$$

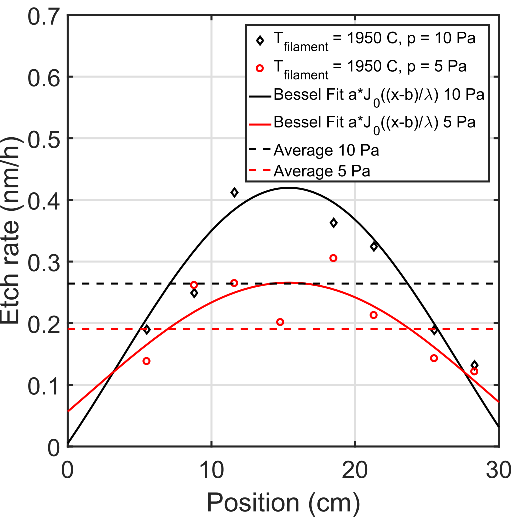

FIG. 6. The carbon etch rate under atomic hydrogen exposure measured at different positions along the VUV beam light path. The markers represent experimental data and are fitted with a first order Bessel function of the first kind.

where L represents the integration length along the beam path and $v_{th} = \sqrt{8k_BT/\pi m}$ is the thermal velocity of the atomic hydrogen species. The carbon etch rate profile, $ER(x)$ in Eq. (9), is presented in Fig. 6. These data are fitted using the radial part of Eq. (6). In Fig. 6, the dashed lines represent averaged etch rates derived by solving the left-hand side of Eq. (9) with the fitted function as input. Together with the line-integrated density obtained using VUV absorption spectroscopy, Eq. (9) can be solved to derive the etching yield.

In this cross calibration, the HRG is used to generate atomic hydrogen. Again, the HRG is operated at 1900 °C. VUV spectroscopy measurements were performed at two moments in time: at the beginning of the exposure and at the end. The results are presented in Table II. An average erosion yield of $Y = (2.04 \pm 1.04) \cdot 10^{-5}$ for an atomic hydrogen flux of 10^{17} cm^{-2} s^{-1} is found using $M_C = 12.0107$ g mol^{-1},[42] $T = 350$ K, and $\rho_C = 2.267 \cdot 10^{-6}$ g m^{-3}[42] for graphite-like carbon. The obtained erosion yield matches the erosion yield reported by Crijns,[21] where a yield of $Y = (2.05 \pm 0.77) \cdot 10^{-5}$ is observed for an atomic hydrogen flux of $3 \cdot 10^{16}$ up to $3 \cdot 10^{17}$ cm^{-2} s^{-1}. This was measured with a heat flux sensor in a hydrogen radical only environment generated using an HRG. In the work of Crijns,[21] carbon samples from the same supplier and manufactured in the same manner are used.

VII. MEASURING ATOMIC HYDROGEN FLUXES IN A H_2 PLASMA ENVIRONMENT

Ultimately, the etching sensor (collective: carbon sample and chimney with bend; see Fig. 1) is deployed in a hydrogen plasma environment to measure atomic hydrogen fluxes. Etching rates are determined using a spectroscopic ellipsometer to measure sample thicknesses pre- and post-exposure. This etch rate is then translated into an atomic hydrogen flux using the erosion yield obtained from cross calibrations discussed earlier in this work. The obtained atomic hydrogen fluxes are compared with heat flux sensor and vacuum ultraviolet absorption spectroscopy measurements. The heat

Published under an exclusive license by AIP Publishing

flux sensor and carbon etching sensor are positioned in the center of the vessel right below the VUV beam path.

As explained, the VUV absorption technique measures a line integrated density, which is translated to a flux using $\Gamma_H = \frac{1}{4} n_c v_{th}$, with n_c being the atomic hydrogen density at the center of the vessel. One requires a density profile in order to spatially resolve the density and derive n_c from the measured line integrated density. As shown before, density profiles are obtained for the hydrogen radical source and are presented in Fig. 6. However, the hydrogen radical sensor tends more toward a point source, whereas the RF plasma source has a broader source region (~175 cm^2); therefore, a flat distribution profile is expected. Possible disturbance of the flat profile by a source term at the vessel wall upon neutralization of hydrogen ions will be neglected since the atomic hydrogen density is assumed much larger than the atomic hydrogen ion density.

The recombination coefficient of the heat flux sensor's detection surface is chosen such that the flux measurement results match the VUV absorption spectroscopy results, as presented in Fig. 7. This results in a recombination coefficient of $\gamma = 0.15$ for atomic hydrogen on platinum, which is consistent with literature values of 0.25 and 0.06 found in Refs. 28 and 25, respectively. It should be noted that variations in recombination coefficients lead to large uncertainties as the atomic hydrogen density measured by using the heat flux sensor is inversely proportional to this number. The heat flux sensor used is described in more detail in the work of Velthuis *et al.*[43]

Measurements of atomic hydrogen fluxes for the different sensors as a function of plasma input power are presented in Fig. 7. For the carbon etching sensor, Eq. (8) is used to translate carbon etch rates to atomic hydrogen fluxes. The experimental results presented in Fig. 7 show, as expected, an increase in atomic hydrogen flux for increasing plasma power for all sensors. Despite the factor 4 discrepancy, similar trends and the same order of magnitude in absolute value are found when comparing the sensing techniques. One potential explanation for this discrepancy lies in the fact that the VUV absorption technique only measures ground state hydrogen radicals, while the carbon etching sensor will measure hydrogen atoms in all excitation states. However, it is expected that only ground state hydrogen atoms will reach the etching samples as the excitation energy is lost upon collision with the chimney wall. The cross calibrated carbon etching efficiency may suffer from this fact in case the plasma and HRG source generate a different excited over ground state hydrogen atom ratio. This can introduce a discrepancy.

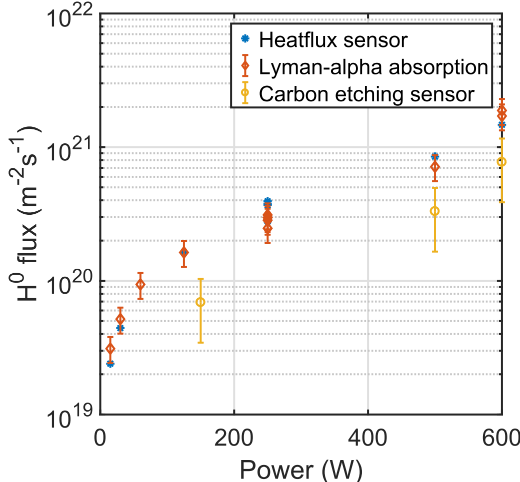

FIG. 7. Atomic hydrogen flux measurements as a function of plasma power at 5 Pa H_2 background pressure for different sensing methods.

At last, in the experimental range used, no issues are expected because of potential reaction product pile-ups. This assumption is based on two observations: (i) a flux-independent (i.e., varying plasma input power) constant factor 4 delta with the other sensing techniques applied. (ii) In Fig. 4, all three datasets are fitted simultaneously using Eq. (6) with the recombination probability as the free fitting parameter. The data fitting goes well for the varying chimney dimensions and thus for varying flows. This suggests that there is no strong dependence on flow variations. To conclude, in the experimental range used in this work, the etching efficiency by etching product pile-ups does not seem to change significantly and could thus be corrected for. This correction will be part of the "chimney transmission" constant.

VIII. CONCLUSION

The carbon etching sensor was successfully deployed in a hydrogen plasma environment. In this work, a radio frequency (13.56 MHz) inductively coupled hydrogen plasma was used as the atomic hydrogen source. This plasma produces ion fluxes of $\Gamma_i \approx 10^{13}$ to 10^{14} cm^{-2} s^{-1} with ion energies of 5–10 eV as measured by using a retarding field energy analyzer for 500 W of plasma power and a H_2 background pressure of 1–10 Pa. It has been demonstrated that the Macor chimney with bend is capable of suppressing the ion flux to an extent that etching of the carbon sample is dominated by atomic hydrogen. The introduction of the bend in the chimney, used to enforce ion–wall collisions, was found to be crucial to further reduce the ion flux to the sample to a point where etching of the carbon sample was governed by atomic hydrogen. Subsequently, the etching sensor was cross calibrated using vacuum ultraviolet absorption spectroscopy, which resulted in an etching yield of $Y = (2.05 \pm 1.04) \cdot 10^{-5}$ for the amorphous carbon sample under atomic hydrogen exposure. This finding is in agreement with literature data. Ultimately, atomic hydrogen fluxes were measured in the plasma environment, and the results were compared with other sensing techniques, such as vacuum ultraviolet absorption spectroscopy, and a heat flux sensor. Atomic hydrogen fluxes of ~10^{17} cm^{-2} s^{-1} are measured. In this setup, the atomic hydrogen flux turned out to be three orders of magnitude higher than the ion flux for the given operation conditions. Still, ion suppression was required by the chimney with bend, showing that hydrogen ions are much more efficient etchers than atomic hydrogen species.

All sensors, i.e., heat flux, VUV absorption spectroscopy, and the carbon etching sensor, measured the atomic hydrogen flux in the plasma environment, and from that, similar trends were observed for all sensing methods. Overall, the developed etching sensor shows within a factor 4 good agreement with other sensing techniques. A recommendation for future work is to check if a varying ratio excited over ground state hydrogen atoms between the HRG and the plasma source could have impacted cross calibrations, which potentially led

Published under an exclusive license by AIP Publishing

to the factor 4 discrepancy. For example, this can be done by using the heat flux sensor as a reference in the cross calibrations to see how the individual sensors align for the two different atomic hydrogen sources. A factor 4 deviation can be accepted in certain applications where the H-flux is a big unknown. For example, in EUV scanners, the H-flux is unknown and being able to quantify this within the given accuracy can already help to mimic offline experimental environments to test plasma–material interactions. Next to that, the etch sensor is simple and can easily be placed anywhere in the EUV scanner. This allows us to determine the atom flux/concentration as a function of position within the EUV scanner. This can be a relative measurement where the constant factor 4 deviation is of less interest.

DATA AVAILABILITY

The data that support the findings of this study are available from ASML Holding. Restrictions apply to the availability of these data, which were used under license for this study. Data are available from the authors upon reasonable request and with the permission of ASML Holding.

REFERENCES

[1] J. P. H. Benschop and V. Banine, "EUV lithography: Main challenges," Proc. SPIE **5401**, 1 (2004).

[2] J. Beckers, T. van de Ven, R. van der Horst, D. I. Astakhov, and V. Banine, "EUV-induced plasma: A peculiar phenomenon of a modern lithographic technology," Appl. Sci. **9**(14), 2827 (2019).

[3] A. Kuznetsov, "Hydrogen particle and plasma interactions with heterogeneous structures," Ph.D. thesis, University of Twente, 2013, p. 10.

[4] M. M. J. W. van Herpen, D. J. W. Klunder, W. A. Soer, R. Moors, and V. Banine, "Sn etching with hydrogen radicals to clean EUV optics," Chem. Phys. Lett. **484**, 197–199 (2010).

[5] A. Dolgov, D. Lopaev, T. Rachimova, A. Kovalev, A. Vasil'eva, C. J. Lee, V. M. Krivtsun, O. Yakushev, and F. Bijkerk, "Comparison of H_2 and He carbon cleaning mechanisms in extreme ultraviolet induced and surface wave discharge plasmas," J. Phys. D: Appl. Phys. **47**(6), 065205 (2014).

[6] A. A. Dolgov, "Plasma-assisted cleaning of extreme UV optics," Ph.D. thesis, University of Twente, The Netherlands, 2018, p. 3.

[7] T. H. M. van de Ven, P. Reefman, E. A. Osorio, V. Y. Banine, and J. Beckers, "Investigation of ion energy distribution functions in EUV-induced plasmas by ion mass spectrometry," in *2016 IEEE International Conference on Plasma Science (ICOPS)* (IEEE, 2016), p. 1.

[8] A. A. Abrikosov, O. F. Yakushev, D. V. Lopaev, and V. M. Krivtsun, "Dynamics of the ion energy spectrum in EUV-induced hydrogen plasma," Plasma Phys. Rep. **43**(06), 614 (2017).

[9] T. H. M. van de Ven, P. Reefman, C. A. de Meijere, R. M. van der Horst, M. van Kampen, V. Y. Banine, and J. Beckers, "Ion energy distributions in highly transient EUV induced plasma in hydrogen," J. Appl. Phys. **123**(6), 063301 (2018).

[10] R. M. van der Horst, J. Beckers, E. A. Osorio, and V. Y. Banine, "Dynamics of the spatial electron density distribution of EUV-induced plasmas," J. Phys. D: Appl. Phys. **48**, 432001 (2015).

[11] R. M. van der Horst, J. Beckers, S. Nijdam, and G. M. W. Kroesen, "Exploring the temporally resolved electron density evolution in extreme ultra-violet induced plasmas," J. Phys. D: Appl. Phys. **47**(30), 302001 (2014).

[12] D. I. Astakhov, W. J. Goedheer, C. J. Lee, V. V. Ivanov, V. M. Krivtsun, K. N. Koshelev, D. V. Lopaev, R. M. van der Horst, J. Beckers, E. A. Osorio, and F. Bijkerk, "Exploring the electron density in plasma induced by EUV radiation: II. Numerical studies in argon and hydrogen," J. Phys. D: Appl. Phys. **49**(29), 295204 (2016).

[13] J. Beckers, F. M. J. H. van de Wetering, B. Platier, M. A. W. van Ninhuijs, G. J. H. Brussaard, V. Y. Banine, and O. J. Luiten, "Mapping electron dynamics in highly transient EUV photon-induced plasmas: A novel diagnostic approach using multi-mode microwave cavity resonance spectroscopy," J. Phys. D: Appl. Phys. **52**(3), 034004 (2018).

[14] G. C. Stutzin, A. T. Young, A. S. Schlachter, J. W. Stearns, K. N. Leung, W. B. Kunkel, G. T. Worth, and R. R. Stevens, "Atomic hydrogen density measurements in an ion source plasma using a VUV absorption spectrometer," Rev. Sci. Instrum. **59**(8), 1479–1481 (1988).

[15] A. T. Young, G. C. Stutzin, P. Chen, W. B. Kunkel, and K. N. Leung, "Measurement of atomic and molecular hydrogen in a tandem magnetic multi-cusp H ion source by VUV spectroscopy," Rev. Sci. Instrum. **63**(4), 2744–2746 (1992).

[16] R. Zaplotnik, A. Vesel, and M. Mozetic, "A fiber optic catalytic sensor for neutral atom measurements in oxygen plasma," Sensors **12**(4), 3857–3867 (2012).

[17] M. Mozetič, M. Drobnič, A. Pregelj, and K. Zupan, "Determination of density of hydrogen atoms in the ground state," in *Proceedings of the 13th International Vacuum Congress and the 9th International Conference on Solid Surfaces* [Vacuum **47**(6), 943–945 (1996)].

[18] M. Mrkvičková, J. RáheǏ, P. Dvořák, D. Trunec, and T. Morávek, "Fluorescence (TALIF) measurement of atomic hydrogen concentration in a coplanar surface dielectric barrier discharge," Plasma Sources Sci. Technol. **25**(5), 055015 (2016).

[19] P. Dvorák, M. Talába, A. Obrusník, J. Kratzer, and J. Dědina, "Concentration of atomic hydrogen in a dielectric barrier discharge measured by two-photon absorption fluorescence," Plasma Sources Sci. Technol. **26**(8), 085002 (2017).

[20] O. V. Braginsky, A. S. Kovalev, D. V. Lopaev, E. M. Malykhin, T. V. Rakhimova, A. T. Rakhimov, A. N. Vasilieva, S. M. Zyryanov, K. N. Koshelev, V. M. Krivtsun, M. van Kaampen, and D. Glushkov, "Removal of amorphous C and Sn on Mo:Si multilayer mirror surface in hydrogen plasma and afterglow," J. Appl. Phys. **111**(9), 093304 (2012).

[21] V. M. C. Crijns, Hydrogen atom based tin cleaning, https://research.tue.nl/en/studentTheses/hydrogen-atom-based-tin-cleaning, 2014.

[22] C. M. Donnelly, R. W. McCullough, and J. Geddes, "Etching of graphite and diamond by thermal energy hydrogen atoms," Diamond Relat. Mater. **6**(5), 787–790 (1997).

[23] B. N. Khare, M. Meyyappan, J. Kralj, P. Wilhite, M. Sisay, H. Imanaka, J. Koehne, and C. W. Baushchlicher, "A glow-discharge approach for functionalization of carbon nanotubes," Appl. Phys. Lett. **81**(27), 5237–5239 (2002).

[24] B. J. Wood and H. Wise, "Diffusion and heterogeneous reaction. II. catalytic activity of solids for hydrogen atom recombination," J. Chem. Phys. **29**, 1416–1417 (1958).

[25] G. A. Melin and R. J. Madix, "Energy accommodation during hydrogen atom recombination on metal surfaces," Trans. Faraday Soc. **67**, 2711–2719 (1971).

[26] D. B. Sheen, "Adsorption and recombination of hydrogen atoms on glass surfaces. Part 1. Method of study and the mechanism of recombination at 77 and 273 k," J. Chem. Soc., Faraday Trans. 1 **75**, 2439–2453 (1979).

[27] Y. C. Kim and M. Boudart, "Recombination of oxygen, nitrogen, and hydrogen atoms on silica: Kinetics and mechanism," Langmuir **7**(12), 2999–3005 (1991).

[28] B. J. Wood and H. Wise, "The kinetics of hydrogen atom recombination on pyrex glass and fused quartz," J. Phys. Chem. **66**(6), 1049–1053 (1962).

[29] R. K. Grubbs and S. M. George, "Attenuation of hydrogen radicals traveling under flowing gas conditions through tubes of different materials," J. Vac. Sci. Technol. A **24**(3), 486–496 (2006).

[30] M. Green, K. R. Jennings, J. W. Linnett, and D. Schofield, "Recombination of atoms at surfaces. Part 7. Hydrogen atoms at silica and other similar surfaces," Trans. Faraday Soc. **55**, 2152–2161 (1959).

[31] G. A. Curley, L. Gatilova, S. Guilet, S. Bouchoule, G. S. Gogna, N. Sirse, S. Karkari, and J. P. Boot, "Surface loss rates of H and Cl radicals in an inductively coupled plasma etcher derived from time-resolved electron density and optical emission measurements," J. Vac. Sci. Technol. A **28**(2), 360–372 (2010).

[32] K. E. Shuler and K. J. Laidler, "The kinetics of heterogeneous atom and radical reactions. I. The recombination of hydrogen atoms on surfaces," J. Chem. Phys. **17**(12), 1212–1217 (1949).

[33] M. Schlüter, C. Hopf, T. Schwarz-Selinger, and W. Jacob, "Temperature dependence of the chemical sputtering of amorphous hydrogenated carbon films by hydrogen," J. Nucl. Mater. **376**(1), 33–37 (2008).

Published under an exclusive license by AIP Publishing

[34]J.-S. Yoon, M.-Y. Song, J.-M. Han, S. H. Hwang, W.-S. Chang, B. Lee, and Y. Itikawa, "Cross sections for electron collisions with hydrogen molecules," J. Phys. Chem. Ref. Data **37**(2), 913–931 (2008).
[35]J. Zalc, S. C. Reyes, and E. Iglesia, "The effects of diffusion mechanism and void structure on transport rates and tortuosity factors in complex porous structures," Chem. Eng. Sci. **59**, 2947–2960 (2004).
[36]G. L. Vignoles, "Modelling binary, Knudsen and transition regime diffusion inside complex porous media," J. Phys. IV Colloq. **05**(C5), C5-159–C5-166 (1995).
[37]M. Knudsen, "Die gesetze der molekularströmung und der inneren reibungsströmung der gase durch röhren," Ann. Phys. **333**(1), 75–130 (1909).
[38]E. H. Kennard, "The kinetic theory of gases. With an introduction to statistical mechanics," J. Soc. Chem. Ind. **57**(39), 901 (1938).
[39]I. Langmuir, "The dissociation of hydrogen into atoms. III. The mechanism of the reaction," J. Am. Chem. Soc. **38**(6), 1145–1156 (1916).
[40]T. Okumura, "Inductively coupled plasma sources and applications," Phys. Res. Int. **2010**, 1.
[41]See https://wwwh.innovationservices.pilips.com for Philips innovation services.
[42]J. S. Coursey, D. J. Schwab, J. J. Tsai, and R. A. Dragoset, Atomic Weights and Isotopic Compositions (version 4.1), 2015, URL: http://physics.nist.gov/Comp.
[43]J. F. M. Velthuis, A. Storm, M. van Kampen, R. van der Horst, and H. B. Profijt, "Radical recombination sensor based on dual probe thermopile heat flux sensors," J. Vac. Sci. Technol. A **37**, 061302 (2019).

Published under an exclusive license by AIP Publishing